ACS NANO

Article

An Oxide Schottky Junction Artificial Optoelectronic Synapse

Shuang Gao, Gang Liu, Huali Yang, Chao Hu, Qilai Chen, Guodong Gong, Wuhong Xue, Xiaohui Yi, Jie Shang, and Run-Wei Li

ACS Nano, **Just Accepted Manuscript** • Publication Date (Web): 07 Feb 2019

Just Accepted

ACS Publications

is published by the American Chemical Society. 1155 Sixteenth Street N.W., Washington, DC 20036

An Oxide Schottky Junction Artificial Optoelectronic Synapse

Shuang Gao,[†,‡] Gang Liu,[,†,‡] Huali Yang,[†,‡] Chao Hu,[†,‡] Qilai Chen,[†,‡] Guodong Gong,[†,‡] Wuhong Xue,[†,‡] Xiaohui Yi,[†,‡] Jie Shang,[†,‡] and Run-Wei Li*[,†,‡]*

[†]*CAS Key Laboratory of Magnetic Materials and Devices, Ningbo Institute of Materials Technology and Engineering, Chinese Academy of Sciences, Ningbo, Zhejiang 315201, China*

[‡]*Zhejiang Province Key Laboratory of Magnetic Materials and Application Technology, Ningbo Institute of Materials Technology and Engineering, Chinese Academy of Sciences, Ningbo, Zhejiang 315201, China*

ABSTRACT: The rapid development of artificial intelligence techniques and future advanced robot systems sparks emergent demand on the accurate perception and understanding of the external environments *via* visual sensing systems that can co-locate the self-adaptive detecting, processing and memorizing of optical signals. In this contribution, a simple indium-tin oxide/Nb-doped $SrTiO_3$ (ITO/Nb:$SrTiO_3$) heterojunction artificial optoelectronic synapse is proposed and demonstrated. Through the light and electric field co-modulation of the Schottky barrier profile at the ITO/Nb:$SrTiO_3$ interface, the oxide heterojunction device can respond to the entire visible light region in a neuromorphic manner, allowing synaptic paired-pulse facilitation, short/long-term memory and "learning-experience" behavior for optical information manipulation. More importantly, the photo-plasticity of the artificial synapse has been modulated by hetero-synaptic means with a sub-1 V external voltage, not only enabling an optoelectronic analog of the mechanical aperture device showing adaptive and stable optical perception capability under different illuminating conditions, but also making the artificial synapse suitable for the mimicry of interest-modulated human visual memories.

KEYWORDS: *oxide heterojunction, Schottky junction, artificial synapse, visual memory, optoelectronic device*

Nearly 80% of the information that human beings receive from the external world is obtained through visual perception.[1] The diverse photodetectors that can convert light stimuli into electrical signals are the extension of human vision and help us to better perceive the world.[2–4] With the rapid development of artificial intelligence techniques and future advanced robot systems that can work under diverse environmental conditions, superior and smart photo-detecting gadgets are urgently desired to enhance and eventually to replace human vision in scientific, industrial and military scenarios. An ideal humanoid photodetector should be responsive in the entire visible spectral coverage with extra high sensitivity, as well as possess certain feedback and control mechanisms to realize self-adaptive response under varied illuminating intensities.[5] Additional *in-situ* neuromorphic computing capabilities will be a plus when handling broadband data-intensive tasks.[6] Nonetheless, the nowadays state-of-the-art photodetectors are usually passive and un-adjustable,[2–4] resulting possibly in the difficulty of high-efficiency signal sensing in an extremely wide optical strength range. The real-time information processing and storage requirements also impose a technical challenge on the traditional volatile photodetector devices at the moment.

The latest confirmation of memristor as the forth fundamental circuit element offers a great opportunity for realizing high-performance neuromorphic computing, wherein the continuous evolution of device conductivity allows the integration of information processing and storage in a single cell by emulating the physiological behavior of biological synapses.[7–14] Very recently, scientists started the attempts of integrating volatile photodetectors with nonvolatile storage devices, with the aim to memorize the detected images.[6,15–17] The combination of an

In_2O_3 nanowire photodetector with an Al_2O_3 memristor has been made to mimic the human visual system.[17] To further eliminate the power-hungry von Neumann communication bottleneck caused by physically separated data processing and memorizing units,[18] our group had employed light-sensitive cerium oxide to construct a multifunctional optoelectronic memristor that can co-locate the detecting, processing and memorizing functions for optical signals.[19,20] Even though, the adaptive response, which is enabled by the iris in the human visual system to prevent the retina from being damaged under strong illumination and to make objects recognizable under weak light,[5] is only achieved in mechanical aperture devices by emulating the control of pupil opening by sphincter and dilator muscles to stabilize the light intensity received by the retina.[21–23] Despite being functional, these aperture devices are complicated in structure and need high operating voltages of dozens to hundreds of volts, thus incompatible with the pure CMOS integrated circuits. Taking all these into account, there is emerging necessity to develop a simple yet effective artificial humanoid optoelectronic device that can integrate the adaptive perception, processing and memorizing functions of optical information.

In this work, we propose and demonstrate a simple indium-tin oxide/Nb-doped $SrTiO_3$ (ITO/Nb:$SrTiO_3$) heterojunction artificial optoelectronic synapse, which exhibits self-adaptive optical signal detecting and integrated information processing and memorizing functions in a single optoelectronic cell. Through continuously modulating the energy band structure and conductance of the ITO/Nb:$SrTiO_3$ heterojunction through the interfacial charge trapping states, the all-oxide artificial synapse demonstrates neuromorphic characteristics of

paired-pulse facilitation (PPF), short- and long-term memory (STM and LTM) as well as "learning-experience" behavior, allowing the *in-situ* processing of the optical signal over the entire visible spectrum. More importantly, its photoresponsive efficiency can be flexibly manipulated by sub-1 V voltage stimuli, enabling an optoelectronic analog of the mechanical aperture device showing adaptive and stable optical perception capability under different illuminating conditions. With these characteristics, the all-oxide heterojunction artificial synapse demonstrates promising suitability for the mimicry of human visual memory, in particular the interest-modulated visual memory effect.

RESULTS AND DISCUSSION

Previous documents indicate that the charge trapping sites at metal oxide surfaces and interfaces play an important role in determining their electrical behaviors.[24–26] By controlling the electron density in the cerium oxide film near the CeO_{2-x}/AlO_y interface with optical illumination, the band diagram at the $CeO_{2-x}/AlO_y/Al$ junction region can be effectively modified to facilitate the charge transport across it, thus giving rise to the persistent photoconductivity characteristics in the ITO/CeO_{2-x}/AlO_y/Al device.[19,20] As inspired, we further simplify the device structure in the present study, by only retaining two conductive oxide layers to form the prerequisite charge trapping interface (Figure 1). Herein, ITO and Nb:$SrTiO_3$ are intentionally selected due to their outstanding transparent conducting feature and rich surface defects for electron trapping/de-trapping,[25–27] respectively. Noting that the electron affinity of Nb:$SrTiO_3$ is ~3.9 eV and its Fermi level is located slightly below the conduction band bottom due to heavy Nb doping (0.7 wt.%),[28,29] together with the high work

function of ITO (~4.5 eV),[30] a Schottky barrier is naturally expected to exist at the ITO/Nb:$SrTiO_3$ interface (Figure 1a). This should make the heterojunction stay in a high resistance state as the large barrier height/width can significantly suppress the tunneling leakage current. Upon light illumination, the trapped electrons in the interfacial defects (mostly, oxygen vacancies[25]) will be released, leaving behind some positively charged empty traps that can provide an additional potential and thus reduces the build-in electric field needed to maintain the Fermi level balance between ITO and Nb:$SrTiO_3$.[24] Consequently, the barrier height/width will become lower/narrower, increasing the probability for electron tunneling and thus switching the heterojunction into a low resistance state (Figure 1c).

In order to experimentally deomstrate the speculated photoresponsive mechanism as well as to evaluate the optoelectrical behavior of the ITO/Nb:$SrTiO_3$ heterojunction, ITO electrodes were deposited directly using pulsed laser deposition (PLD) technique on commercially available Nb:$SrTiO_3$ (100) single-crystalline substrate with a thickness of 0.5 mm and a Nb doping content of 0.7 wt.%. During deposition, a metal shadow mask was used to pattern the ITO electrode to be circular with a diameter of 100 μm. With the designed thickness of 100 nm, the as-deposited ITO electrode is highly transparent with an average transmittance of up to ~88% in the wavelength region of 400~700 nm (Figure S1, Supporting Information). Cross-sectional transmission electron microscope (TEM) analysis confirms a clear ITO/Nb:$SrTiO_3$ heterojunction interface (Figure S2, Supporting Information). For optoelectrical measurements, two source measurement units (SMUs) were involved, wherein SMU1 with the help of a power amplifier is used to drive a light emitting diode (LED) for the

introduction of optical stimuli onto the heterojunction, while SMU2 is mainly for electrical stressing and conductance measurements (Figure S3, Supporting Information). In this case, the optical and electrical stimuli were able to be independently and arbitrarily programmed. Capacitance measurements were conducted first on the heterojunction before and after 100 s bule light (459 nm, Figure S4, Supporting Information) exposure with an intensity of 30 mW/cm^2. The obtained results reveal a clear capacitance increase after light exposure (Figure S5, Supporting Information), which can well support the speculated photoresponsive mechanism in Figure 1 when considering the fact that heterojunction capacitance is inversely proportional to the barrier width.[24]

Basic photoresponsive characteristics of the ITO/Nb:$SrTiO_3$ heterojunction artificial optoelectronic synapse are provided in Figure 2. A typical current evolution process of the heterojunction under 0.05 V read voltage and upon bule light exposure with an intensity of 30 mW/cm^2 is seen in Figure 2a. The continuous illumination of 100 s can result in a notable current change (ΔI) of 55 nA, followed by a gradual decay when the light is off. The decay process should result from the metastability of empty traps, which can be gradually neutralized by capturing electrons from the conduction band of Nb:$SrTiO_3$.[31,32] The fitting result in Figure 2b indicates that the current decay process accords well with the Kohlrausch stretched-exponential function[33]

$$I_t = \Delta I \cdot \exp(-(t/\tau)^{\beta}) + I_C \quad (1)$$

where τ and β denote the relaxation time constant and the stretching exponent, respectively, while I_C represents the background current of 30 nA. The τ is fitted to be ~1.2×10^4 s and thus

suggests a good nonvolativity of the photoresponsive characteristic, as confirmed by the retention results of >3000 s in Figure S6 (Supporting Information). As for the β, it is fitted to be ~0.20, which coincides well with the previously reported values for two-dimensional electron systems[31,34] and thus can support as well the proposed interfacial (rather than fillamentary) photoresponsive mechanism in Figure 1. To better reveal its photoresponsive characteristics, the heterojunction was then exposed to blue light stimuli with various periods and intensities. The obtained results in Figure 2c suggest that a larger ΔI can be casued by either a longer illuminating time or a higher light intensity. Moreover, it is found that the heterojunction is able to respond not only to blue light but also to green and red ones, as illustrated in Figure 2d. Herein, all the lights used have the same intensity of 30 mW/cm^2, and the detailed wavelengths of green and red lights are 528 nm and 630 nm, reapectively (Figure S4, Supporting Information). Apparently, the heterojunction is more sensitive to light illumination with a shorter wavelength, possibly due to a higher external quantum yield.[35]

Besides continuous optical stressing, pulsed light stimuli have also been applied to the ITO/Nb:$SrTiO_3$ heterojunction. What is interesting is that the obtained photoresponsive results can be processed by the heterojunction in typical neuromorphic manners, as shown in Figure 3. First of all, a series of blue light pulse pairs with varied interval (Δt) values were applied to the heterojunction, wherein all pulses had a width of 0.5 s and an intensity of 30 mW/cm^2. Figure 3a shows the measured result for Δt = 0.5 s, which clearly demonstrates a much higher photoresponsive current evoked by the second light pulse. If using A_1 and A_2 to

denote the amplitudes of photoresponsive currents evoked respectively by the first and second light pulses, the A_2/A_1 is found to decay with Δt following a double-exponential function

$$A_2/A_1 = 1 + C_1 \cdot \exp(-\Delta t/\tau_1) + C_2 \cdot \exp(-\Delta t/\tau_2) \quad (2)$$

where C_1 (C_2) and τ_1 (τ_2) are the initial facilitation magnitude and the characteristic relaxation time of the rapid (slow) decay term, respectively (Figure 3b). These behaviors remind us of the common and important synaptic plasticity called paired-pulse facilitation (PPF), which is essential to recognize and decode temporal information like visual and auditory signals in a biological neural system.[36,37] Specifically, PPF describes the fact that a second pre-synaptic spike will normally cause an enhanced post-synaptic current than the first one in biological synapses, while the enhancement extent is closely related to the time interval between these two spikes. As such, the heterojunction can be reasonably regarded as an artificial optoelectronic synapse, with the input light pulse, heterojunction conductance and photoresponsive current as the pre-synaptic spike, synaptic weight and post-synaptic current, respectively. Moreover, it is obtained by fitting that τ_1 = 3.86 s and τ_2 = 41.0 s for the heterojunction. Apparently, τ_2 is about one order of magnitude larger than τ_1, which agrees well with the measured data in biological synapses.[38]

In psychology there are two types of memory behaviors, *i.e.*, short- and long-term memory (STM and LTM), both of which are considered to result from the synaptic plasticity.[35,39,40] The STM is stored in the hippocampus and corresponds to the temporal weak potentiation of synaptic weight, which persists only for a few seconds or minutes and then fades away almost completely. After repetitive rehearsal named consolidation, the STM will be transferred into

the cerebral cortex as the LTM, which corresponds to the permanent strong potentiation of synaptic weight that lasts from hours to years, or even a lifetime.[41] Using pulsed light stimuli with varied number (*n*) or frequency (*f*), STM, LTM as well as STM-to-LTM transition have been well demonstrated in the ITO/Nb:$SrTiO_3$ heterojunction artificial optoelectronic synapse, as shown in Figure 3c and 3d. Obviously, with an increase in *n* or *f*, the potentiation of synaptic weight has gradually changed from weak (*i.e.*, STM) to strong (*i.e.*, LTM). Also, the current decay time and the steady current after decay have been confirmed to increase with *n* or *f* (Figure S7, Supporting Information). These accord well with the STM-to-LTM transition in human brains.[40,42,43] Meanwhile, the interesting "learning-experience" behavior of human brains has also been demonstrated, as presented in Figure 3e. Herein, two light pulse trains with an interval of 100 s were successively used to stimulate the heterojunction. The synaptic weight was notably potentiated by the first pulse train and then decayed spontaneously to an intermediate level in the train interval, analogous to the phenomenon that the learned information by a person tends to be partially forgotten after a period of time. To recover the decayed synaptic weight, only 7 pulses in the second stimulating process were found to be enough, which is far fewer than the 35 pulses needed in the first stimulating process to cause an identical potentiation of synaptic weight. Also, within the same period of 100 s, the decay in synaptic weight after the second stimulating process is found to be much smaller than that after the first stimulating process. Such behaviors resemble the facts that less time is usually required by a person to relearn the lost information that has been previosly memorized, and that the relearning process can significantly strengthen the memory stability.[37] It is noted that

all memory effects can be completely erased through the neutralization of empty traps induced by a negaitve voltage (Figure S8, Supporting Information),[24] which makes our heterojunction artificial optoelectronic synapse able to be easily revitalized. Moreover, good uniformity and reliability have been confirmed in our heterojunction device (Figure S8 and S9, Supporting Information).

With the integrated optical information detecting, processing and memorizing capabilities, the ITO/Nb:$SrTiO_3$ heterojunction artificial optoelectronic synapse has been demonstrated to be versatile for the mimicry of human visual memory. Experimentally, nine heterojunction synapses were randomly chosen from a single wafer to recognize and memorize the input images consisting of 3×3 pixels, and each was stimulated by a fixed period of 100 s (pulse width, 0.5 s; frequency, 0.5 or 1 Hz) with the predefined pixel color and intensity, followed by the decay measurement of post-synaptic current at 0.05 V for 100 s. Figure 4a shows the obtained result for an input image encoded by light wavelength. Apparently, the input image has been well recognized through the post-synaptic current contrast and reliably memorized for a long time period. Similar result has also been found for an input image encoded by light intensity, as illustrated in Figure 4b. Besides, for the same input image, a lower stimulating frequency will naturally lead to a weaker memory effect, as confirmed in Figure 4c.

More importantly, we found that photoresponsive efficiency of the ITO/Nb:$SrTiO_3$ heterojunction can be flexibly modulated by applying an external voltage (V_m) to the ITO electrode, as shown in Figure 5a. Experimentally, the heterojunction was exposed to 100 s

bule light with an intensity of 30 mW/cm^2 and simultaneously stressed by various V_m values. It is clear that the photoresponsive efficiency has been notably enhanced and suppressed by positive and negative V_m values, respectively. As such, by setting appropriate V_m values, photoresponsive results of the heterojunction under different exposure conditions can be modulated to be identical, as demonstrated in Figure 5b. This characteristic very much resembles the function of iris in human eyes, which can stabilize the visual effect in various light environments through adjusting the pupil size.[5] Under consecutive optical pulses, voltage gating of the junction photo-plasticity can also be confirmed (Figure 5c), which is actually the hetero-synaptic plasticity that is considered to be essential for a large number of key biological functions like associative learning.[44] As for the modulation mechanism, electric field-induced oxygen migration as well as electron trapping/de-trapping has been considered, as shown schematically in Figure 1. When $V_m > 0$ V, it can cause the out-diffusion of oxygen ions from Nb:$SrTiO_3$ to ITO and thus the formation of additional oxygen vacancies at the interface.[45,46] Upon light illumination, part of these oxygen vacancies can also become positively charged through light-induced de-trapping of electrons. Meanwhile, the positive V_m itself can directly cause the de-trapping of electrons from oxygen vacancies to some extent.[24] These factors together result in the existence of more oxygen vacancies, in particular the positively charged ones at the jucntion interface, thus making the barrier height/width to be lower/narrower than that for $V_m = 0$ V, *i.e.*, enhanced photoresponsive efficiency (Figure 1b). On the contrary, a negative V_m will cause the migration of oxygen ions from ITO to Nb:$SrTiO_3$ as well as the trapping of electrons by

already positively charged oxygen vacancies,[24,45,46] which finally lead to fewer oxygen vacancies (especially the positively charged ones) at the junction interface than that for $V_m = 0$ V, *i.e.*, suppressed photoresponsive efficiency (Figure 1d). It is noted that V_m should be no larger than ~0.4 V to ensure that the contribution of V_m itself to the total current change is minor (Figure S10, Supporting Information). Also, it should not be too negative because breakdown of the heterojunction will occur at ~-4 V (Figure S11, Supporting Information).

With the above V_m-modulated photoresponsive efficiency, an advanced function of human visual memory has been well mimicked, as shown in Figure 5d and Figure S12 (Supporting Information). In detail, V_m is used to modulate the visual memory effect, which resembles the fact that real visual memory is normally affected by many other factors, such as personal interest, mood, attention, *etc*.[47] Herein, let us assume that a person has a low, intermediate and high interest to the letter "L", "I" and "H", respectively. If so, after an identical viewing time, the person will certainly get a weak to strong memory for the input images in the panels (i) to (iii), respectively. As expected, such behavior has been well mimicked by simply using V_m = -0.15 V, 0 V and 0.15 V to represent respectively the low, intermediate and high interest signals, wherein the visual memory system increase their output intensity accordingly (Figure 5d and Figure S8). These results promise wide applications of our artificial optoelectronic synapse in future electronic eyes, multifunctional robotics, intelligent sensors, *etc*.

Before concluding, a detailed comparison between previously reported photoelectronic artificial memristive synapses[43,48–51] and our ITO/Nb:$SrTiO_3$ heterojunction one is provided in

Table 1. It is clear that our device has the simplest bilayer structure, together with a wide light-responsive region and a moderate light-responsive intensity. More importantly, the voltage-modulated photo-plasticity as well as the "learning-experience" behavior is demonstrated exclusively in our device, which likely promises it a wider application scope. Meanwhile, due to an improved Schottky barrier property, the heavy metal/Nb:$SrTiO_3$ heterojunction has been confirmed to exhibit a better resistive switching performance (such as lower leakage current and higher ON/OFF ratio) when the memory cell is scaled down to nanoscale.[52] As such, with the same interfacial charge trapping/de-trapping mechanism, a good miniaturization potential can be expected in our ITO/Nb:$SrTiO_3$ heterojunction artificial optoelectronic synapse. Moreover, the photo-response speed could be improved by increasing the work function of ITO (for example, through crystallinity optimization and chlorine doping[53,54]) or by replacing ITO with graphene that is also transparent and conductive but with a slightly higher work function of ~4.7 eV.[55] This is because a larger work function difference can theoretically cause a higher built-in electric field at the heterojunction, which will accelerate the separation between photo-excited electrons and empty traps and thus result in a faster photo-response speed.[20]

CONCLUSIONS

A simple ITO/Nb:$SrTiO_3$ heterojunction artificial optoelectronic synapse was proposed and fabricated, which can respond to the entire visible light region in a partially nonvolatile manner and with a higher sensitivity to the shorter wavelength. Theoretical analysis and capacitance measurement confirm the photoresponsive mechanism to be light-induced

de-trapping of electrons from interfacial defects. More importantly, the photoresponsive efficiency can be flexibly modulated by applying a sub-1 V external voltage, and the photoresponsive results can be *in-situ* processed following typical neuromorphic manners, such as PPF, STM, LTM, STM-to-LTM transition and "learning-experience" behavior. These characteristics together make the heterojunction artificial synapse highly suited for the mimicry of human visual memory, especially the interest-modulated visual memory effect.

EXPERIMENTAL SECTION

Device Fabrication. The device fabrication process was started with a commercially available Nb:$SrTiO_3$ (100) single-crystalline substrate (HEFEI KEJING MATERIALS TECHNOLOGY CO., LTD), which is 5×5×0.5 mm^3 in size with one side polished and has a Nb doping content of 0.7 wt.%. The ITO electrodes with a thickness of 100 nm and a diameter of 100 μm were deposited on the polished side of the substrate by PLD with the help of a metal shadow mask. The detailed deposition parameters were 248 nm laser wavelength, 75 mJ pulse energy, 1 Hz repetition rate, 0.8 Pa oxygen pressure, and room temperature. The device fabrication process was ended with the covering of silver paste on the other side of the substrate to ensure ohmic contact during subsequent electrical measurements.

Device Characterization. A focused ion beam (FIB) system (Auriga, Carl Zeiss) was used to fabricate the cross-sectional specimen, which was then examined by a TEM (Tecnai F20, FEI). The optical transmittance of the ITO electrode was measured using a UV-VIS-NIR spectrometer (Lambda 950, Perkin Elmer). The spectra of all LEDs were recorded by a fluorescence spectrometer (FL3-111, Horiba), while their illumination intensities were

calibrated using a light meter (Li-250A, LI-COR). The capacitance measurement was done by an impedance analyzer (1260A, Solartron) with 0.05 V DC and AC voltage signals, whereas all the other electrical measurements were conducted using a precision semiconductor parameter analyzer (4200 SCS, Keithley) with 0.05 V read voltage. During all electrical measurements, the sample was put in a home-made dark chamber to exclude the influence of environment lights.

ASSOCIATED CONTENT

Supporting Information is available free of charge on the ACS Publications website at DOI: …

Optical transmittance of the deposited ITO electrode (Figure S1); Cross-sectional TEM analysis of the ITO/Nb:$SrTiO_3$ heterojunction. (Figure S2); Schematic structure with measurement configuration of the ITO/Nb:$SrTiO_3$ heterojunction (Figure S3); Detailed emission spectra of the used blue, green and red LEDs (Figure S4); Light-induced capacitance change of the ITO/Nb:$SrTiO_3$ heterojunction (Figure S5); Retention performance of the ITO/Nb:$SrTiO_3$ heterojunction (Figure S6); The variations of current decay time and steady current after decay during the STM-to-LTM transition (Figure S7); Consecutive 30 cycles of blue light-induced potentiation and negative voltage-induced depression of synaptic weight in the ITO/Nb:$SrTiO_3$ heterojunction (Figure S8); Synaptic plasticity of 10 randomly chosen ITO/Nb:$SrTiO_3$ heterojunction cells (Figure S9); The contribution of the V_m-induced current change to the light-induced current change with V_m enhancement (Figure S10); Breakdown of the

ITO/Nb:$SrTiO_3$ heterojunction under negative voltage sweep (Figure S11); Decay process of the mimicked interest-modulated human visual memory (Figure S12).

The authors declare no competing financial interest.

AUTHOR INFORMATION

Corresponding Authors

*E-mail: liug@nimte.ac.cn.

*E-mail: runweili@nimte.ac.cn.

ORCID

Gang Liu: 0000-0002-3142-9323

Run-Wei Li: 0000-0003-3879-9834

ACKNOWLEDGEMENTS

The authors thank Mr. Yangming Fu and Prof. Liqiang Zhu for their kind help on the capacitance measurement. The authors acknowledge the financial supports from the National Key R&D Program of China (2017YFB0405604), National Natural Science Foundation of China (61704178, 61722407, 61774161, 61674153, 61504154, 51525103 and 11474295), Natural Science Foundation of Zhejiang Province (LR17E020001), Public Welfare Technical Applied Research Project of Zhejiang Province (2017C31100), Ningbo Science and Technology Innovation Team (2015B11001), and Ningbo Natural Science Foundation (2017A610093 and 2018A610020).

REFERENCES

(1) Wang, G.; Wang, R.; Kong, W.; Zhang, J. Simulation of Retinal Ganglion Cell Response Using Fast Independent Component Analysis. *Cogn. Neurodyn.* **2018**, *12*, 615–624.

(2) Ostroverkhova, O. Organic Optoelectronic Materials: Mechanisms and Applications. *Chem. Rev.* **2016**, *116*, 13279–13412.

(3) Ahmadi, M.; Wu, T.; Hu, B. A Review on Organic–Inorganic Halide Perovskite Photodetectors: Device Engineering and Fundamental Physics. *Adv. Mater.* **2017**, *29*, 1605242.

(4) García de Arquer, F. P.; Armin, A.; Meredith, P.; Sargent, E. H. Solution-Processed Semiconductors for Next-Generation Photodetectors. *Nat. Rev. Mater.* **2017**, *2*, 16100.

(5) Lee, G. J.; Choi, C.; Kim, D.-H.; Song, Y. M. Bioinspired Artificial Eyes: Optic Components, Digital Cameras, and Visual Prostheses. *Adv. Funct. Mater.* **2018**, *28*, 1705202.

(6) Wang, H.; Zhao, Q.; Ni, Z.; Li, Q.; Liu, H.; Yang, Y.; Wang, L.; Ran, Y.; Guo, Y.; Hu, W.; Liu, Y. A Ferroelectric/Electrochemical Modulated Organic Synapse for Ultraflexible, Artificial Visual-Perception System. *Adv. Mater.* **2018**, *30*, 1803961.

(7) Strukov, D. B.; Snider, G. S.; Stewart, D. R.; Williams, R. S. The Missing Memristor Found. *Nature* **2008**, *453*, 80–83.

(8) Jo, S. H.; Chang, T.; Ebong, I.; Bhadviya, B. B.; Mazumder, P.; Lu, W. Nanoscale Memristor Device as Synapse in Neuromorphic Systems. *Nano Lett.* **2010**, *10*, 1297–1301.

(9) Prezioso, M.; Merrikh-Bayat, F.; Hoskins, B. D.; Adam, G. C.; Likharev, K. K.; Strukov, D. B. Training and Operation of an Integrated Neuromorphic Network Based on Metal-Oxide Memristors. *Nature* **2015**, *521*, 61–64.

(10) Tuma, T.; Pantazi, A.; Le Gallo, M.; Sebastian, A.; Eleftheriou, E. Stochastic Phase-Change Neurons. *Nat. Nanotechnol.* **2016**, *11*, 693–699.

(11) Wang, Z.; Joshi, S.; Savel'ev, S. E.; Jiang, H.; Midya, R.; Lin, P.; Hu, M.; Ge, N.; Strachan, J. P.; Li, Z.; Wu, Q.; Barnell, M.; Li, G.-L.; Xin, H. L.; Williams, R. S.; Xia, Q.;

Yang, J. J. Memristors with Diffusive Dynamics as Synaptic Emulators for Neuromorphic Computing. *Nat. Mater.* **2016**, *16*, 101–108.

(12) Najem, J. S.; Taylor, G. J.; Weiss, R. J.; Hasan, M. S.; Rose, G.; Schuman, C. D.; Belianinov, A.; Collier, C. P.; Sarles, S. A. Memristive Ion Channel-Doped Biomembranes as Synaptic Mimics. *ACS Nano* **2018**, *12*, 4702–4711.

(13) Zhang, Y.; He, W.; Wu, Y.; Huang, K.; Shen, Y.; Su, J.; Wang, Y.; Zhang, Z.; Ji, X.; Li, G.; Zhang, H.; Song, S.; Li, H.; Sun, L.; Zhao, R.; Shi, L. Highly Compact Artificial Memristive Neuron with Low Energy Consumption. *Small* **2018**, *14*, 1802188.

(14) Choi, S.; Tan, S. H.; Li, Z.; Kim, Y.; Choi, C.; Chen, P.-Y.; Yeon, H.; Yu, S.; Kim, J. SiGe Epitaxial Memory for Neuromorphic Computing with Reproducible High Performance Based on Engineered Dislocations. *Nat. Mater.* **2018**, *17*, 335–340.

(15) Nau, S.; Wolf, C.; Sax, S.; List-Kratochvil, E. J. W. Organic Non-Volatile Resistive Photo-Switches for Flexible Image Detector Arrays. *Adv. Mater.* **2015**, *27*, 1048–1052.

(16) Wang, H.; Liu, H.; Zhao, Q.; Ni, Z.; Zou, Y.; Yang, J.; Wang, L.; Sun, Y.; Guo, Y.; Hu, W.; Liu, Y. A Retina-Like Dual Band Organic Photosensor Array for Filter-Free Near-Infrared-to-Memory Operations. *Adv. Mater.* **2017**, *29*, 1701772.

(17) Chen, S.; Lou, Z.; Chen, D.; Shen, G. An Artificial Flexible Visual Memory System Based on an UV-Motivated Memristor. *Adv. Mater.* **2018**, *30*, 1705400.

(18) Backus, J. Can Programming be Liberated from the von Neumann Style? A Functional Style and Its Algebra of Programs. *Commun. ACM* **1978**, *21*, 613–641.

(19) Tan, H.; Liu, G.; Zhu, X.; Yang, H.; Chen, B.; Chen, X.; Shang, J.; Lu, W. D.; Wu, Y.; Li, R.-W. An Optoelectronic Resistive Switching Memory with Integrated Demodulating and Arithmetic Functions. *Adv. Mater.* **2015**, *27*, 2797–2803.

(20) Tan, H.; Liu, G.; Yang, H.; Yi, X.; Pan, L.; Shang, J.; Long, S.; Liu, M.; Wu, Y.; Li, R.-W. Light-Gated Memristor with Integrated Logic and Memory Functions. *ACS Nano* **2017**, *11*, 11298–11305.

(21) Draheim, J.; Burger, T.; Korvink, J. G.; Wallrabe, U. Variable Aperture Stop Based on the Design of a Single Chamber Silicone Membrane Lens with Integrated Actuation. *Opt. Lett.* **2011**, *36*, 2032–2034.

(22) Schuhladen, S.; Preller, F.; Rix, R.; Petsch, S.; Zentel, R.; Zappe, H. Iris-Like Tunable Aperture Employing Liquid-Crystal Elastomers. *Adv. Mater.* **2014**, *26*, 7247–7251.

(23) Schuhladen, S.; Banerjee, K.; Stürmer, M.; Müller, P.; Wallrabe, U.; Zappe, H. Variable Optofluidic Slit Aperture. *Light Sci. Appl*. **2016**, *5*, e16005.

(24) Yan, Z. B.; Liu, J. M. Coexistence of High Performance Resistance and Capacitance Memory Based on Multilayered Metal-Oxide Structures. *Sci. Rep.* **2013**, *3*, 2482.

(25) Yin, X.-B.; Tan, Z.-H.; Guo, X. The Role of Schottky Barrier in the Resistive Switching of $SrTiO_3$: Direct Experimental Evidence. *Phys. Chem. Chem. Phys.* **2015**, *17*, 134–137.

(26) Fan, Z.; Fan, H.; Yang, L.; Li, P.; Lu, Z.; Tian, G.; Huang, Z.; Li, Z.; Yao, J.; Luo, Q.; Chen, C.; Chen, D.; Yan, Z.; Zeng, M.; Lu, X.; Gao, X.; Liu, J.-M. Resistive Switching Induced by Charge Trapping/Detrapping: a Unified Mechanism for Colossal Electroresistance in Certain Nb:$SrTiO_3$-Based Heterojunctions. *J. Mater. Chem. C* **2017**, *5*, 7317–7327.

(27) Park, J.; Kwon, D.-H.; Park, H.; Jung, C. U.; Kim, M. Role of Oxygen Vacancies in Resistive Switching in Pt/Nb-doped $SrTiO_3$. *Appl. Phys. Lett.* **2014**, *105*, 183103.

(28) Robertson, J. Band Offsets of Wide-Band-Gap Oxides and Implications for Future Electronic Devices. *J. Vac. Sci. Technol. B* **2000**, *18*, 1785–1791.

(29) Cui, Y.; Liu, W.; Wang, R. Visible Light Initiated and Collapsed Resistive Switching in $TbMnO_3$/Nb:$SrTiO_3$ Heterojunctions. *Phys. Chem. Chem. Phys.* **2013**, *15*, 6804–6808.

(30) Park, Y.; Choong, V.; Gao, Y.; Hsieh, B. R.; Tang, C. W. Work Function of Indium Tin Oxide Transparent Conductor Measured by Photoelectron Spectroscopy. *Appl. Phys. Lett.* **1996**, *68*, 2699–2701.

(31) Hu, W. J.; Paudel, T. R.; Lopatin, S.; Wang, Z.; Ma, H.; Wu, K.; Bera, A.; Yuan, G.; Gruverman, A.; Tsymbal, E. Y.; Wu, T. Colossal X-Ray-Induced Persistent Photoconductivity in Current-Perpendicular-to-Plane Ferroelectric/Semiconductor Junctions. *Adv. Funct. Mater.* **2018**, *28*, 1704337.

(32) Lany, S.; Zunger, A. Anion Vacancies as a Source of Persistent Photoconductivity in II-VI and Chalcopyrite Semiconductors. *Phys. Rev. B* **2005**, *72*, 035215.

(33) Phillips, J. C. Stretched Exponential Relaxation in Molecular and Electronic Glasses. *Rep. Prog. Phys.* **1996**, *59*, 1133–1207.

(34) Li, J. Z.; Lin, J. Y.; Jiang, H. X.; Khan, M. A.; Chen, Q. Persistent Photoconductivity in a Two-Dimensional Electron Gas System Formed by an AlGaN/GaN Heterostructure. *J. Appl. Phys.* **1997**, *82*, 1227–1230.

(35) Lee, M.; Lee, W.; Choi, S.; Jo, J.-W.; Kim, J.; Park, S. K.; Kim, Y.-H. Brain-Inspired Photonic Neuromorphic Devices Using Photodynamic Amorphous Oxide Semiconductors and Their Persistent Photoconductivity. *Adv. Mater.* **2017**, *29*, 1700951.

(36) Hu, S. G.; Liu, Y.; Chen, T. P.; Liu, Z.; Yu, Q.; Deng, L. J.; Yin, Y.; Hosaka, S. Emulating the Paired-Pulse Facilitation of a Biological Synapse with a NiO_x-Based Memristor. *Appl. Phys. Lett.* **2013**, *102*, 183510.

(37) Liu, G.; Wang, C.; Zhang, W.; Pan, L.; Zhang, C.; Yang, X.; Fan, F.; Chen, Y.; Li, R.-W. Organic Biomimicking Memristor for Information Storage and Processing Applications. *Adv. Electron. Mater.* **2016**, *2*, 1500298.

(38) Zucker, R. S.; Regehr, W. G., Short-Term Synaptic Plasticity. *Annu. Rev. Physiol.* **2002**, *64*, 355–405.

(39) Atkinson, R. C.; Shiffrin, R. M. Human Memory: A Proposed System and Its Control Processes. *Psychol. Learn. Motiv. - Adv. Res. Theory* **1968**, *2*, 89–195.

(40) Wang, Z. Q.; Xu, H. Y.; Li, X. H.; Yu, H.; Liu, Y. C.; Zhu, X. J. Synaptic Learning and Memory Functions Achieved Using Oxygen Ion Migration/Diffusion in an Amorphous InGaZnO Memristor. *Adv. Funct. Mater.* **2012**, *22*, 2759–2765.

(41) Li, S.; Zeng, F.; Chen, C.; Liu, H.; Tang, G.; Gao, S.; Song, C.; Lin, Y.; Pan, F.; Guo, D. Synaptic Plasticity and Learning Behaviours Mimicked Through Ag Interface Movement in an Ag/Conducting Polymer/Ta Memristive System. *J. Mater. Chem. C* **2013**, *1*, 5292–5298.

(42) Chang, T.; Jo, S.-H.; Lu, W. Short-Term Memory to Long-Term Memory Transition in a Nanoscale Memristor. *ACS Nano* **2011**, *5*, 7669–7676.

(43) He, H.-K.; Yang, R.; Zhou, W.; Huang, H.-M.; Xiong, J.; Gan, L.; Zhai, T.-Y.; Guo, X. Photonic Potentiation and Electric Habituation in Ultrathin Memristive Synapses Based on Monolayer MoS_2. *Small* **2018**, *14*, 1800079.

(44) Yang, Y.; Yin, M.; Yu, Z.; Wang, Z.; Zhang, T.; Cai, Y.; Lu, W. D.; Huang, R. Multifunctional Nanoionic Devices Enabling Simultaneous Heterosynaptic Plasticity and Efficient In-Memory Boolean Logic. *Adv. Electron. Mater.* **2017**, *3*, 1700032.

(45) Baeumer, C.; Raab, N.; Menke, T.; Schmitz, C.; Rosezin, R.; Müller, P.; Andrä, M.; Feyer, V.; Bruchhaus, R.; Gunkel, F.; Schneider, C. M.; Waser, R.; Dittmann, R. Verification of Redox-Processes as Switching and Retention Failure Mechanisms in Nb:$SrTiO_3$/Metal Devices. *Nanoscale* **2016**, *8*, 13967–13975.

(46) Cooper, D.; Baeumer, C.; Bernier, N.; Marchewka, A.; La Torre, C.; Dunin-Borkowski, R. E.; Menzel, S.; Waser, R.; Dittmann, R. Anomalous Resistance Hysteresis in Oxide ReRAM: Oxygen Evolution and Reincorporation Revealed by *In Situ* TEM. *Adv. Mater.* **2017**, *29*, 1700212.

(47) Lamme, V. A. F. Why Visual Attention and Awareness are Different. *Trends Cogn. Sci.* **2003**, *7*, 12–18.

(48) Jaafar, A. H.; Gray, R. J.; Verrelli, E.; O'Neill, M.; Kelly, S. M.; Kemp, N. T. Reversible Optical Switching Memristors with Tunable STDP Synaptic Plasticity: a Route to Hierarchical Control in Artificial Intelligent Systems. *Nanoscale* **2017**, *9*, 17091–17098.

(49) Hu, D.-C.; Yang, R.; Jiang, L.; Guo, X. Memristive Synapses with Photoelectric Plasticity Realized in ZnO_{1-x}/AlO_y Heterojunction. *ACS Appl. Mater. Interfaces* **2018**, *10*, 6463–6470.

(50) Tan, H.; Ni, Z.; Peng, W.; Du, S.; Liu, X.; Zhao, S.; Li, W.; Ye, Z.; Xu, M.; Xu, Y.; Pi, X.; Yang, D. Broadband Optoelectronic Synaptic Devices Based on Silicon Nanocrystals for Neuromorphic Computing. *Nano Energy* **2018**, *52*, 422–430.

(51) Kumar, M.; Abbas, S.; Kim, J. All-Oxide-Based Highly Transparent Photonic Synapse for Neuromorphic Computing. *ACS Appl. Mater. Interfaces* **2018**, *10*, 34370–34376.

(52) Hou, J.; Nonnenmann, S. S.; Qin, W.; Bonnell, D. A. Size Dependence of Resistive Switching at Nanoscale Metal-Oxide Interfaces. *Adv. Funct. Mater.* **2014**, *24*, 4113–4118.

(53) Oh, W.-K.; Hussain, S. Q.; Lee, Y.-J.; Lee, Y.; Ahn, S.; Yi, J. Study on the ITO Work Function and Hole Injection Barrier at the Interface of ITO/a-Si:H(p) in Amorphous/Crystalline Silicon Heterojunction Solar Cells. *Mater. Res. Bull.* **2012**, *47*, 3032–3035.

(54) Helander, M. G.; Wang, Z. B.; Qiu, J.; Greiner, M. T.; Puzzo, D. P.; Liu, Z. W.; Lu, Z. H. Chlorinated Indium Tin Oxide Electrodes with High Work Function for Organic Device Compatibility. *Science* **2011**, *332*, 944–947.

(55) Shi, Y.; Kim, K. K.; Reina, A.; Hofmann, M.; Li, L.-J.; Kong, J. Work Function Engineering of Graphene Electrode *via* Chemical Doping. *ACS Nano* **2010**, *4*, 2689–2694.

Figure 1. Schematic operation mechanism of the ITO/Nb:$SrTiO_3$ heterojunction artificial optoelectronic synapse. (a) Initial Schottky barrier profile. (b) Schottky barrier profile after light illumination accompanied by positive voltage stress. (c) Schottky barrier profile after only light illumination. (d) Schottky barrier profile after light illumination accompanied by negative voltage stress. The dashed lines in (b-d) represent the initial energy band profile.

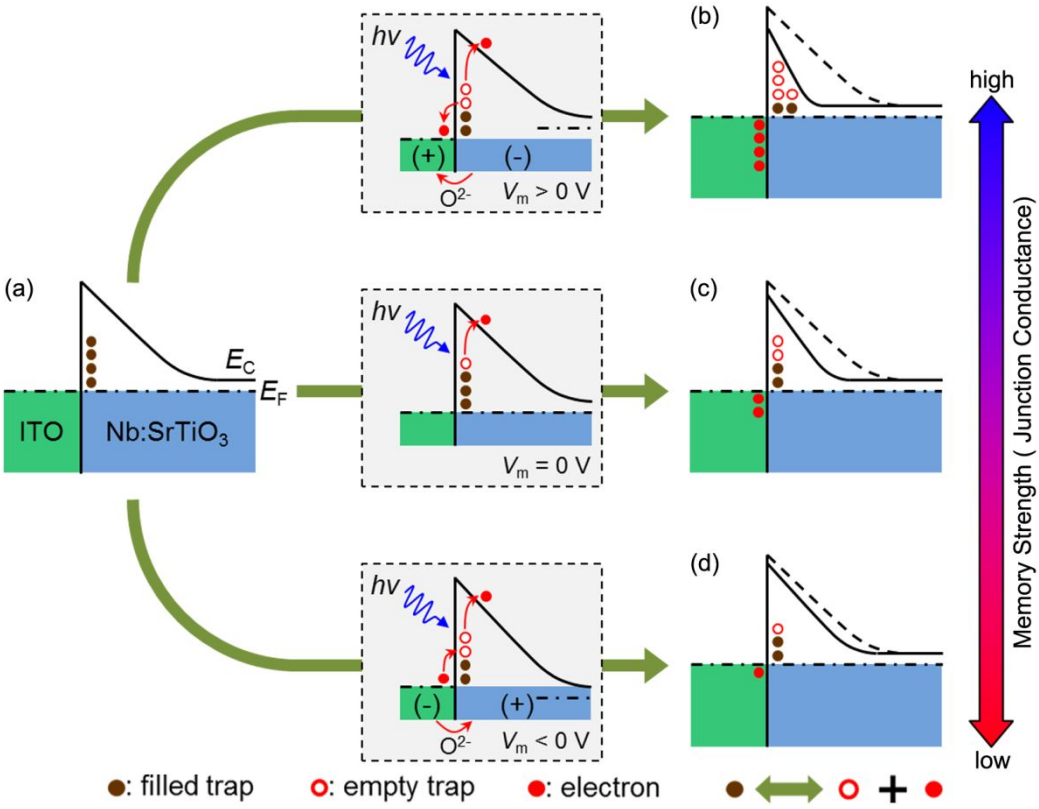

Figure 2. Basic photoresponsive characteristics of the ITO/Nb:$SrTiO_3$ heterojunction artificial optoelectronic synapse. (a) Typical current evolution process of the heterojunction under blue light with an intensity of 30 mW/cm^2. (b) Fitting result of the current decay region in (a). Current changes of the heterojunction (c) under blue light with different intensities and (d) under lights with various colors but an identical intensity of 30 mW/cm^2.

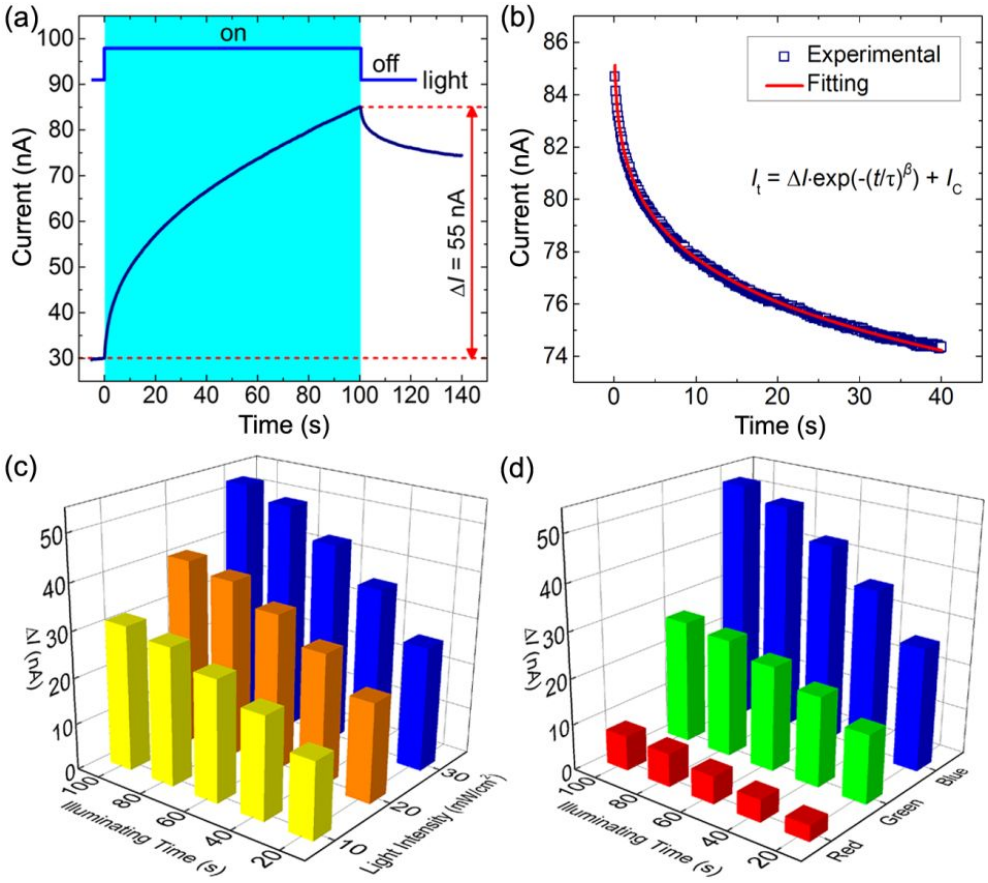

Figure 3. Photoresponsive characteristics of the ITO/Nb:$SrTiO_3$ heterojunction artificial optoelectronic synapse under pulsed light stimuli. (a) Typical photoresponsive characteristic of the heterojunction under a light pulse pair with 0.5 s interval. (b) The variation of PPF index with the interval of light pulse pairs. The STM-to-LTM transition induced by increasing the (c) number or (d) frequency of pulsed light stimuli. (e) The measured "learning-experience" behavior under pulsed light stimuli. Light pulse: color, blue; intensity, 30 mW/cm^2; width, 0.5 s. Pulse frequency in (c,e): 1 Hz.

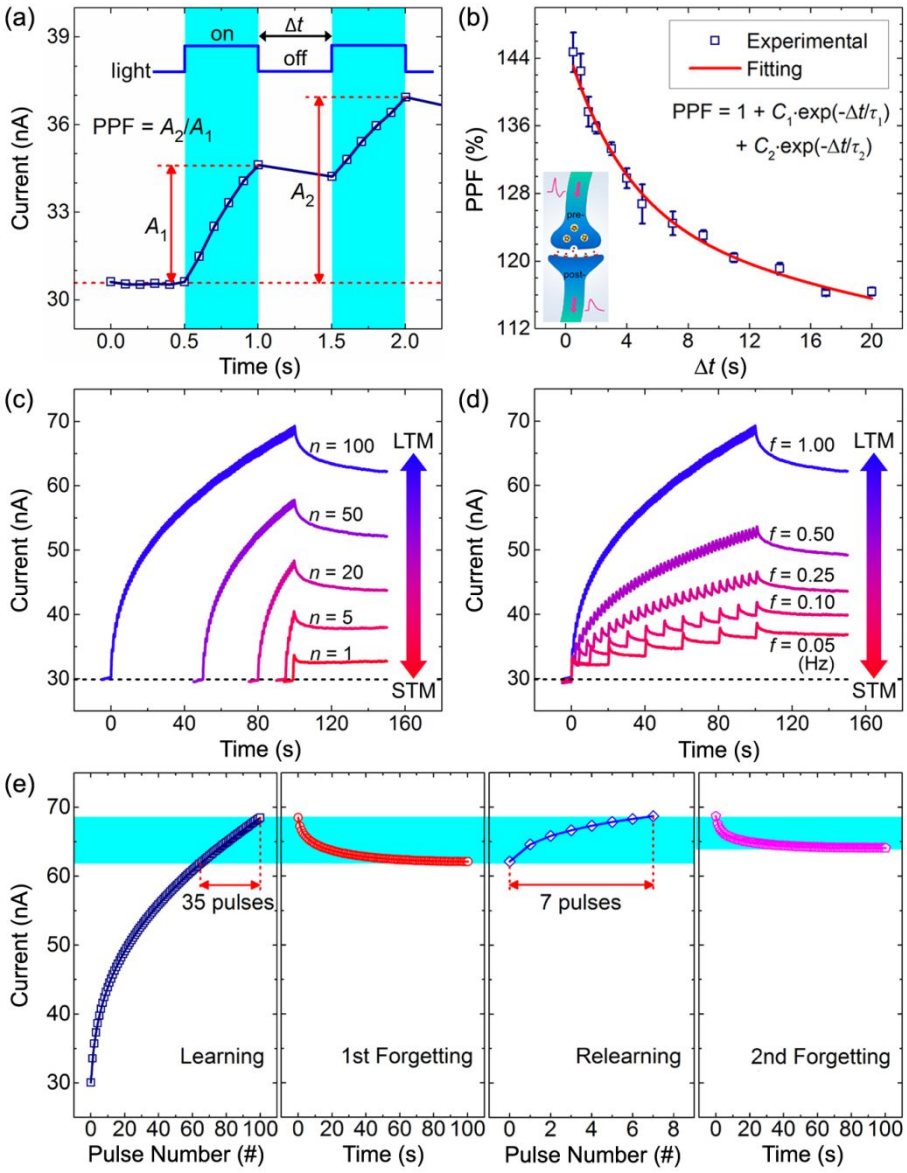

Figure 4. The mimicry of human visual memory using the ITO/Nb:$SrTiO_3$ heterojunction artificial optoelectronic synapse. (a) Input image encoded by light wavelength with stimulating frequency of 1Hz. Input image encoded by light intensity with stimulating frequency of (b) 1 Hz and (c) 0.5 Hz.

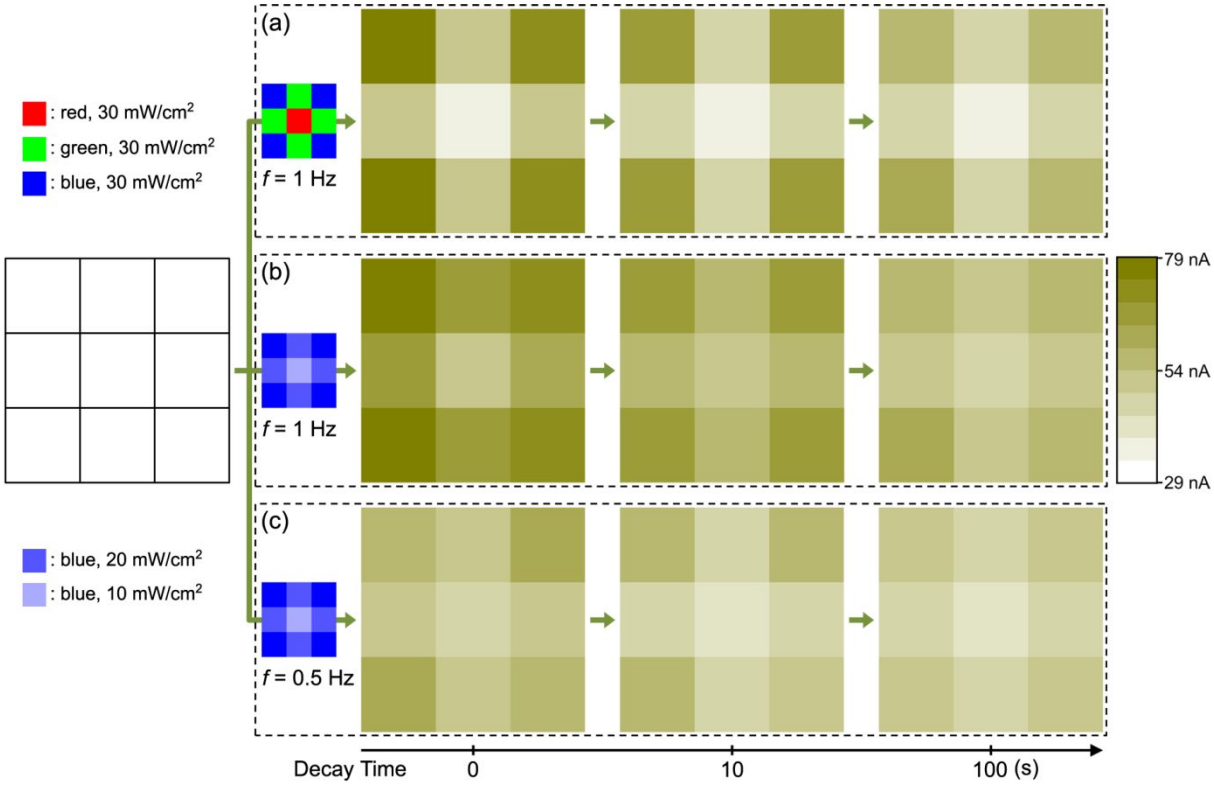

Figure 5. External voltage-modulated photoresponsive efficiency of the ITO/Nb:$SrTiO_3$ heterojunction artificial optoelectronic synapse and its application for the mimicry of interest-modulated human visual memory. (a) External voltage-modulated photoresponsive efficiency. Light: color, blue; intensity, 30 mW/cm^2; illuminating time, 100 s. V_m: stressing time, 100 s. (b) Identical photoresponsive result obtained by setting appropriate external voltages for various illuminating conditions. Light: illuminating time, 100 s. V_m: stressing time, 100 s. (c) External voltage-modulated synaptic plasticity. Light pulse: color, blue; intensity, 30 mW/cm^2; width, 0.5 s; frequency, 1 Hz. V_m pulse: width, 0.5 s; frequency, 1 Hz. (d) The mimicry of interest-modulated human visual memory with (i) low interest represented by V_m = -0.15 V, (ii) intermediate interest represented by V_m = 0 V, and (iii) high interest represented by V_m = 0.15 V. Light pulse: width, 0.5 s; frequency, 1 Hz; number, 100. V_m pulse: width, 0.5 s; frequency, 1 Hz; number, 100.

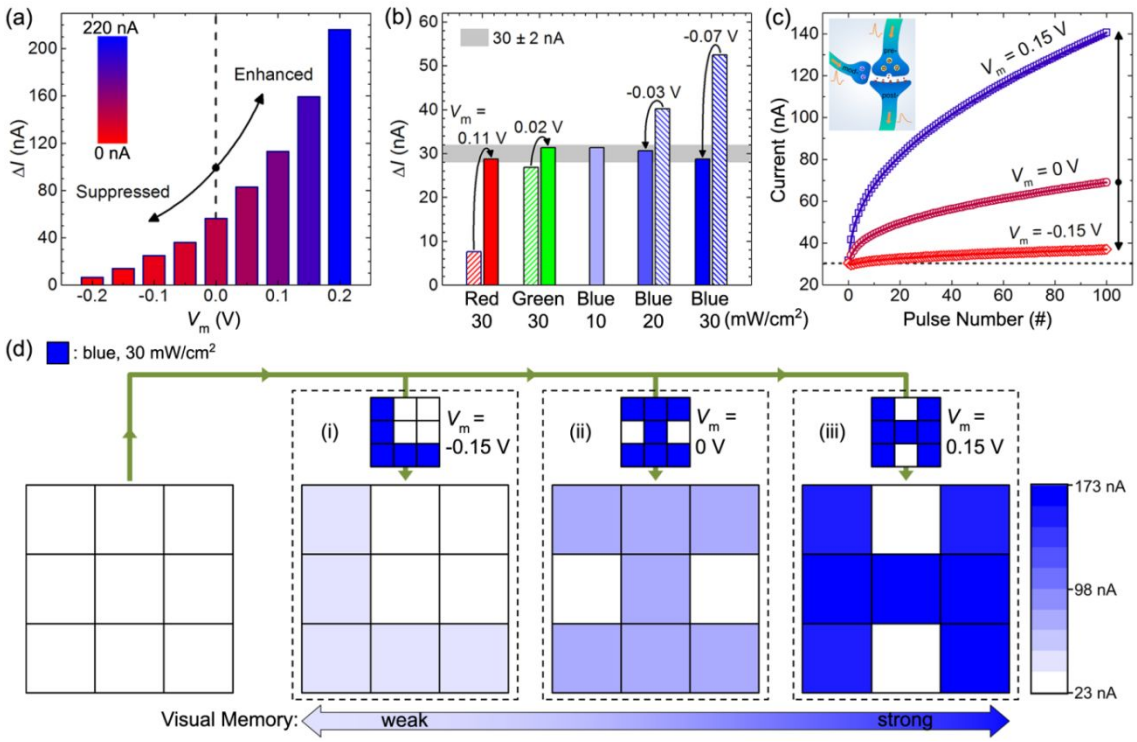

Table 1. The comparison between previous artificial photoelectronic memristive synapses and this work. Symbols "√" and "–" denote demonstrated and non-demonstrated synaptic functions, respectively.

device structure	light source	light intensity (mW/cm^2)	PPF	STM-to-LTM transition	learning-experience behavior	voltage-modulated plasticity
ITO/ZnO/PDR1A/Al[48]	Green	180	–	√	–	–
ITO/ZnO_{1-x}/AlO_y/Al[49]	UV[a)]	~0.072	√	√	–	–
W/MoS_2/SiO_2/p-Si[43]	UV	0.12	√	√	–	–
ITO/Si-NC/Al[50]	UV-NIR[b)]	~18	√	√	–	–
FTO/ZnO/In_2O_3/Au[51]	UV	0.4	√	√	–	–
ITO/Nb:$SrTiO_3$ (this work)	Vis[c)]	10~30	√	√	√	√

[a)]UV: ultraviolet; [b)]NIR: near-infrared; [c)]Vis: visible region

Graphical Table of Contents: